Journal of Luminescence 169 (2016) 627–634

Contents lists available at ScienceDirect

Journal of Luminescence

journal homepage: www.elsevier.com/locate/jlumin

Ion beam induced luminescence studies of sol gel derived Y_2O_3:Dy^{3+} nanophosphors

N.J. Shivaramu [a], K.R. Nagabhushana [b,*], B.N. Lakshminarasappa [a], Fouran Singh [c]

[a] Department of Physics, Jnanabharathi Campus, Bangalore University, Bangalore 560 056, India
[b] Department of Physics (S & H), PES Institute of Technology, 100 feet Ring Road, Banashankari 3rd Stage, Bangalore 560 085, India
[c] Inter University Accelerator Centre, P.O. Box No. 10502, New Delhi 110 067, India

ARTICLE INFO

Article history:
Received 23 September 2014
Received in revised form
20 May 2015
Accepted 24 July 2015
Available online 21 August 2015

Keywords:
Y_2O_3 nanoparticles
Swift heavy ions
Ionoluminescence
Photoluminescence

ABSTRACT

Pure and Dy^{3+} doped Y_2O_3 are prepared by sol–gel technique. The samples are annealed at 900 °C to obtain crystalline phase. X-ray diffraction (XRD) patterns confirm cubic phase of Y_2O_3. The crystallites size is calculated using Scherrer formula and is found to be in the order of 29.67 nm. The particles are found to be spherical in nature and their sizes are estimated to be 35 nm by scanning electron microscope (SEM) technique. Online ionoluminescence (IL) spectra of pure and Dy^{3+} doped Y_2O_3 are recorded with 100 MeV Si^{8+} ions with fluence in the range 0.375–6.75 × 10^{13} ions cm^{-2}. Undoped samples do not show IL emission for any of the fluence explored. Four prominent IL emissions with peaks at 488, 670, 767 nm and a prominent pair at 574 and 584 nm are observed in Dy^{3+} doped samples. These characteristic emissions are attributed to luminescence centers activated by Dy^{3+} ions due to $^4F_{9/2}\rightarrow{}^6H_{15/2}$, $^4F_{9/2}\rightarrow{}^6H_{11/2}$, $^4F_{9/2}\rightarrow{}^6H_{9/2}+{}^6H_{11/2}$ and $^4F_{9/2}\rightarrow{}^6H_{13/2}$ transitions respectively. Further, it is found that IL intensity at 574 nm decays rapidly with ion fluence. A broad and weak photoluminescence (PL) emission with peak at ~485 nm and a strong emission at 573 nm are observed in ion irradiated Y_2O_3:Dy^{3+}. It is found that PL intensity increases with ion fluence up to 3 × 10^{10} ions cm^{-2} and then it decreases with further increase of ion fluence. This may be attributed to lattice disorder produced by dense electronic excitation under swift heavy ion irradiation.

1. Introduction

Swift heavy ion (SHI) irradiation induce changes in nanostructure materials. The energy deposition on target material is usually expressed in terms of kilo electron volt per atomic mass unit (keV/amu). When an energetic ion penetrates a target, it deposits energy mainly by elastic collision with the nuclei known as nuclear energy loss (S_n), which dominates at lower energy (~10 KeV/amu) and inelastic collisions with the electrons of the target known as electronic energy loss (S_e), which dominates at higher energy region (≥ 1 MeV/amu) [1,2]. SHI irradiation induces defects, defect cluster and large number of electron excitation and ionization in target [3–5]. Yttrium oxide (Y_2O_3) is found to be one of the best hosts for rare earth (RE) ions because of its similarities in the chemical properties and ionic radius. Y_2O_3 possess high melting point (~2600 °C), wide transparency range, high thermal conductivity, high chemical stability with a band gap (5.72 eV) and low cut of phonon energy (380 cm^{-1}), which reduces the multiphonon relaxation process and leads to high luminescence efficiency [6]. Trivalent dysprosium ion (Dy^{3+}) has been extensively studied in various hosts due to its unique spectral properties [7]. Dy^{3+}doped Y_2O_3 exhibit excellent greenish yellow luminescent properties. Y_2O_3:Dy^{3+} nanophosphor used for UV based white light emitting diode (white LED), display devices etc.

Ionoluminescence (IL) is non thermal light emission phenomenon induced by bombardment of high energetic ion beam. It is a sensitive and versatile tool for study of excitation states of the material, local symmetry of the emitting atom, chemical state and presence of RE ions [8]. IL studies have been reported on various types of natural and synthetic inorganic materials [9–12]. The objective of the present work is to study ion induced luminescence characteristics of Y_2O_3:Dy^{3+} nanophosphors.

2. Experimental

2.1. Synthesis

Dysprosium doped yttrium oxide is synthesized by sol gel technique using yttrium oxide [99.8% pure (Y_2O_3), Aldrich chemicals], anhydrous citric acid [99.5% pure GR ($C_6H_8O_7$), Merck

* Corresponding author.
E-mail address: bhushankr@gmail.com (K.R. Nagabhushana).

http://dx.doi.org/10.1016/j.jlumin.2015.07.054
0022-2313/

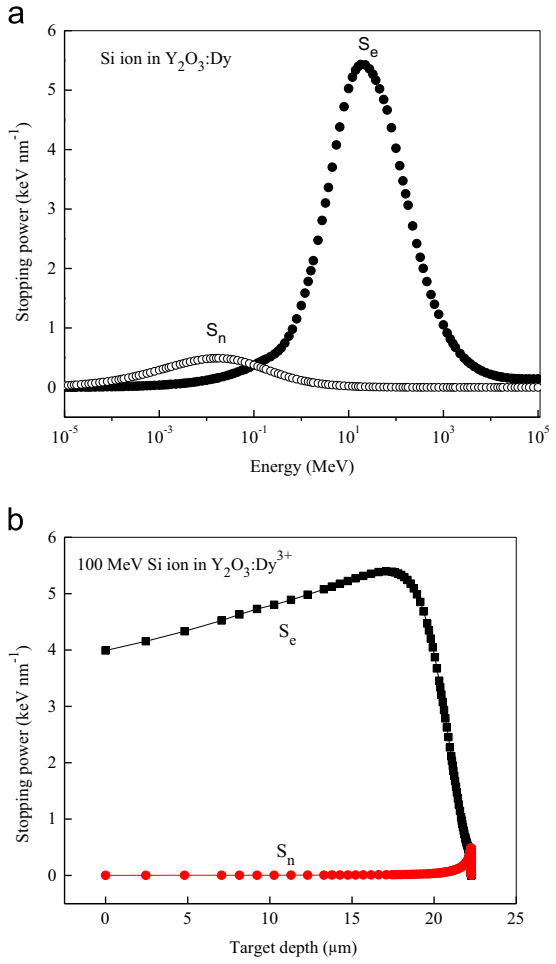

Fig. 1. (a) SRIM graphs for SHI irradiated Y_2O_3:Dy^{3+} nanophosphor and (b) plot of energy loss of 100 MeV Si^{8+} ions in Y_2O_3:Dy^{3+} nanophosphor.

chemicals], dysprosium nitrate [99.9% pure (Dy $(NO_3)_3$), Aldrich chemicals] and nitric acid [(HNO_3), Merck chemicals] as reactants. The ratio of citric acid to Y^{3+} is considered as 2.0 [13,14]. Stoichiometric amount of yttrium oxide is dissolved with dilute nitric acid to get yttrium nitrate and then dissolved in 50 ml of double distilled water. The resultant solution is refluxed at room temperature for 3 h. Dysprosium nitrate is added to yttrium nitrate precursor solution and the solution is again refluxed at 70 °C for 2 h and then citric acid is slowly added to act as a chelating agent. During refluxing, the solution slowly evaporated and turned into a reddish brown gel. The gel is dried at 110 °C in an oven to obtain powder and the powder is grained in an agate mortar and pestle and finally annealed at 700 °C for 2 h to remove the impurities if any [15]. The pellets of 1 mm thick and 5 mm diameter are prepared from 30 mg of the sample by applying a pressure of 4.0 MPa using an homemade pellatizer. 4% of polyvinyl alcohol solution is used as binder [16]. These pellets are annealed at 900 °C for 2 h in a muffle furnace to remove the deformations and binding agent impurities.

2.2. Irradiation

Annealed pellets are irradiated with 100 MeV swift Si^{8+} ions (beam current=2 pnA) for the fluence in the range 1×10^{10}–3×10^{11} ion cm^{-2} using 5 UD Pelletron at Inter University Accelerator Center (IUAC), New Delhi, India [17,18]. The samples are mounted on glass slide of 10 cm length, 2.5 cm width and 2 mm thickness.

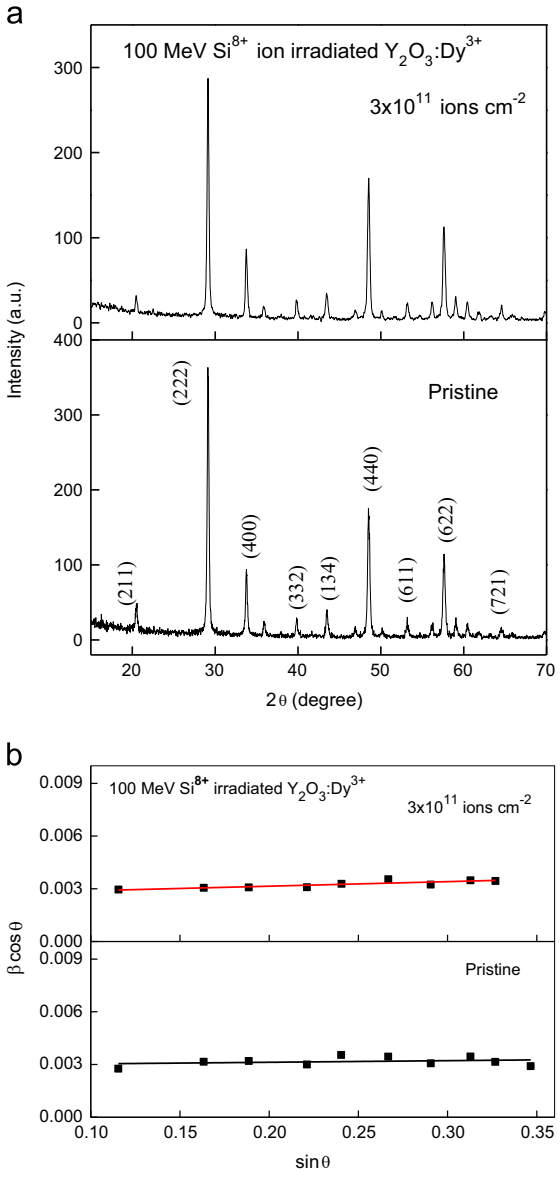

Fig. 2. (a) X-ray diffraction patterns of pristine and 100 MeV swift Si^{8+} ion irradiated Y_2O_3:Dy^{3+} and (b) W–H plot of pristine and 100 MeV swift Si^{8+} ion irradiated Y_2O_3:Dy^{3+}.

Then the slide is carefully fixed on a copper target ladder using double sided tape. The ion beam is magnetically scanned on 1 cm × 1 cm area of the sample surface for uniform irradiation at room temperature. Four pellets are exposed at a time for the same fluence each for XRD, FTIR, PL and thermoluminescence (TL) measurements. IL is performed with focused ion beam inside a high vacuum chamber (6×10^{-6} Torr). The IL emission is collected at 45° to the incident beam and the spectrum recorded using charged coupled device (CCD) camera (Ocean optics spectrometer HR 4000).

2.3. Characterization

XRD patterns are recorded in advanced D-8 X-ray diffractometer (Bruker AXS-model) using 1.5406 Å from Cu K_α radiations. The morphology of the synthesized sample is studied by scanning electron microscopy (JEOL JSM-840A). Fourier transformed infrared spectra (FTIR) are recorded on Nicollet Magna 550 spectrophotometer. PL excitation, emission and the life time

measurements are recorded using an Edinburgh luminescence spectrometer (model F900) equipped with a xenon flash lamp as the source of excitation.

3. Results and discussion

The electronic energy loss (S_e), nuclear energy loss (S_n) and projected ion range (R_p) of Si ions in Y_2O_3:Dy^{3+} are calculated using SRIM (Stopping and Range of Ions in Matter, version 2010) program [19]. S_e and S_n values for 100 MeV Si^{8+} ions are found to be 4.103 and 0.003 keV nm^{-1}, respectively. The projected range of 100 MeV Si^{8+} ions in Y_2O_3:Dy^{3+} is calculated to be 21.65 μm. Fig. 1(a) shows the energy loss (S_e and S_n) as a function of energy for silicon ion in Y_2O_3:Dy^{3+}. Fig. 1(b) shows the variation of energy loss with the penetration depth in the target materials. The electronic energy loss is dominant in the present case and responsible for the material modifications. Thus, it is expected that large electronic excitation may induce breaking of original bonds leading to creation of point defects [20].

Fig. 2(a) shows XRD pattern of pristine and 100 MeV swift Si^{8+} ion irradiated Y_2O_3:Dy^{3+} for the fluence of 3×10^{11} ions cm^{-2}. The XRD pattern of pristine and irradiated samples shows the cubic crystal system with space group $1a\bar{3}$ (JCPDS: No: 88-1040) [21]. All the diffraction peaks have been found to correspond to bixbyite (C-type) crystalline phase of yttrium oxide. It is found that the diffraction peak intensity of irradiated sample decreases when compared to pristine one. This might be due to the creation of large number of defects and discontinuous tracks leading to distortion of crystalline symmetry. Gaboriaud et al., reported SHI irradiation induces phase transformation from cubic to monoclinic structure of yttrium oxide when $S_e \geq 18$ keV nm^{-1} [22]. However, in the present work S_e (4.103 keV nm^{-1}) is much lower and structural phase transformation is not observed instead large numbers of point defects responsible for luminescence are created [23]. Youmei Sun et al., reported the damage induced by SHI in polycarbonate. They reported that the intensity of the main diffraction peak of pristine sample decreases gradually with increasing ion fluence due to destruction of a chemical group [24].

The structural parameters such as miller indices (h k l), crystallite size (D), inter planar spacing (d), lattice constant (a), cell volume (V), density (D_x), dislocation density (δ) and lattice strain (ε) [25] are calculated from XRD data and tabulated in Table 1. The crystallite size (D) is calculated using Scherrer equation:

$$D = \frac{0.9\lambda}{\beta \cos\theta} \quad (1)$$

where, 'λ' is the wavelength of X-rays (1.5406 Å), 'β' is full width at half maxima (FWHM) and 'θ' is the Bragg angle. The average crystallite size is found to be 29.67 nm for pristine while it is 29.00 nm for ion irradiated samples. Significant strains are associated with nanoparticles because a large number of surface atoms have unsaturated in coordination numbers. The lattice strain and

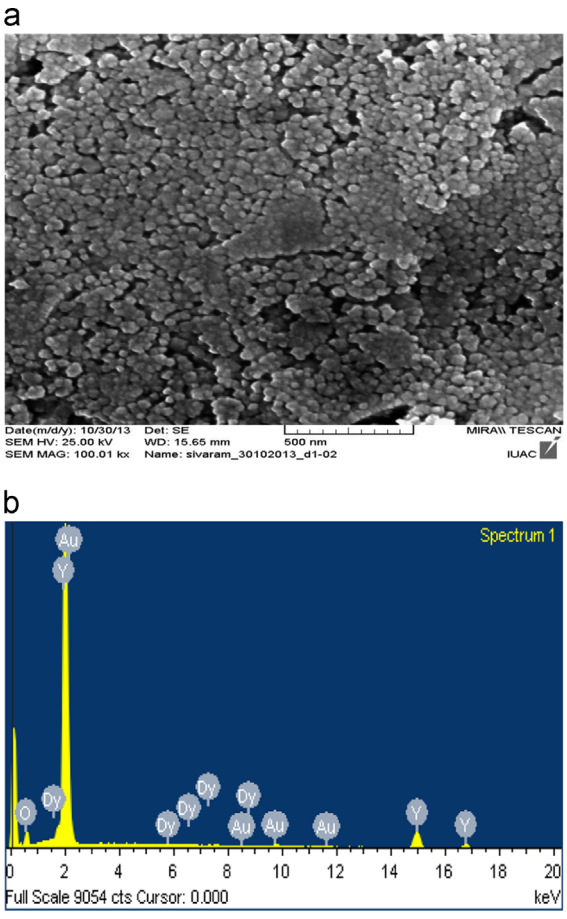

Fig. 3. (a) SEM micrograph of sol gel synthesized nanocrystalline Y_2O_3:Dy^{3+} and (b) EDS of sol gel synthesized nanocrystalline Y_2O_3:Dy^{3+}.

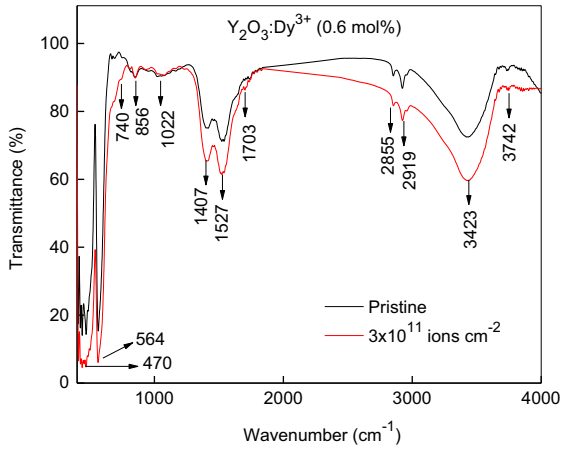

Fig. 4. FTIR spectrum of pristine and 100 MeV swift Si^{8+} ion irradiated Y_2O_3:Dy^{3+}.

Table 1
XRD structural parameters of pristine and 100 MeV swift Si^{8+} irradiated Y_2O_3:Dy^{3+} (Ion fluence: 3×10^{11} ions cm^{-2}).

Y_2O_3:Dy^{3+}	Crystallite size D (nm)		Lattice constant a (Å)	Cell volume (Å^3)	Density ρ (g cm^{-3})	Dislocation density δ ($\times 10^{15}$ m^2)	Inter-planar space in at (222) (Å)	Effective strain (%)	
	Scherrer	W–H method						W–H method	Calculated
Pristine	29.67	37.04	10.597	1190.16	5.042	1.14	3.059	0.045	0.117
3×10^{11} ions cm^{-2}	29.00	36.01	10.593	1188.66	5.047	1.19	3.057	0.090	0.120

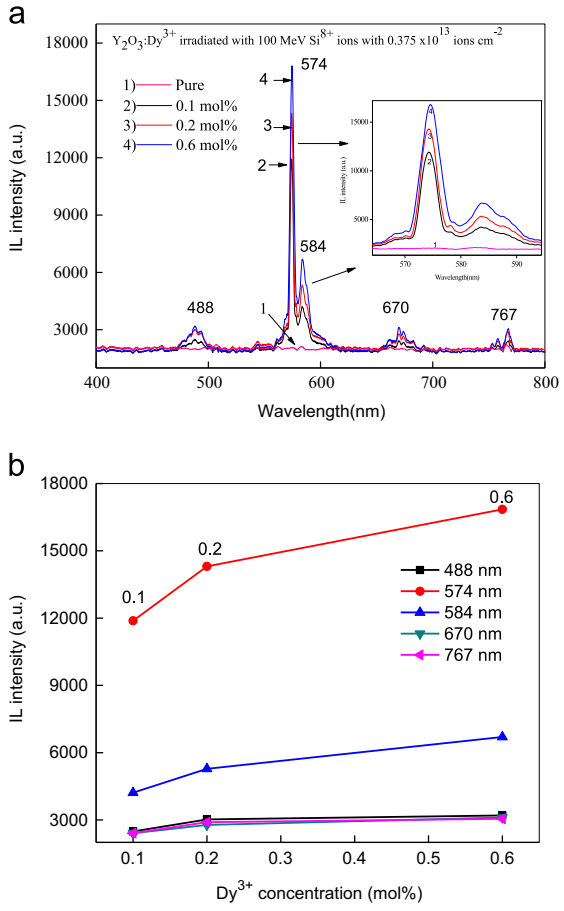

Fig. 5. (a) IL spectra of pure and (0.1 mol%, 0.2 mol% and 0.6 mol%) Dy^{3+} doped Y_2O_3 irradiated with 100 MeV Si^{8+} for fluence of 0.375×10^{13} ions cm^{-2} and (b) variation of IL intensity with Dy^{3+} concentration.

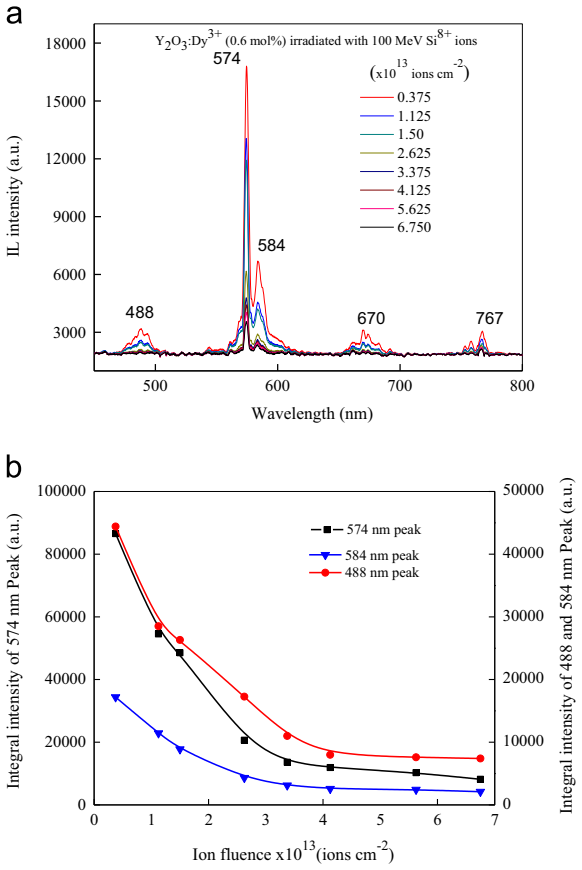

Fig. 6. (a) Ionoluminescence spectra of $Y_2O_3:Dy^{3+}$ irradiated with 100 MeV Si^{8+} ions and (b) variation of IL intensity with ion fluences.

crystallite size are estimated and compared the strains in pristine and SHI irradiated $Y_2O_3:Dy^{3+}$ nanophosphor using Williamson Hall (W–H) method using following equation [26,27]

$$\frac{\beta \, \mathrm{Cos}\, \theta}{\lambda} = \frac{1}{D} + \frac{4\varepsilon \, \mathrm{Sin}\, \theta}{\lambda} \tag{2}$$

where, 'ε' is the lattice strain. Fig. 2(b) represents the plot of $\beta \cos\theta/\lambda$ versus $\sin\theta/\lambda$. The average crystallites size and lattice strain are found to be 37.04 nm and 0.045% for pristine and 36.01 nm and 0.090% for ion irradiated samples.

The dislocation density (δ) is calculated using the following equation [28]

$$\delta = \frac{1}{D^2} \tag{3}$$

where, D is the crystallite size obtained from Scherrer equation. The dislocation density is found to be 1.14×10^{15} m^{-2} for pristine and 1.19×10^{15} m^{-2} for irradiated samples. The increase in lattice strain and dislocation density after SHI irradiation might be due to SHI induced defects in the $Y_2O_3:Dy^{3+}$ nanophosphor [20].

Fig. 3(a) shows the SEM image of heat treated $Y_2O_3:Dy^{3+}$. The SEM picture indicates that the particles are spherical in nature and their size is estimated to be 35 nm. The Energy Dispersive X-ray analysis (EDAX) technique has proved to be a powerful tool to obtain the chemical composition of the sample as shown in Fig. 3 (b). It confirms the presence of Y, O, Dy elements in the synthesized sample.

Fig. 4 shows the FTIR spectra of pristine and SHI irradiated $Y_2O_3:Dy^{3+}$ nanophosphor. The vibrational bands at 470, 564, 740, 856, 1022, 1407, 1527, 1703, 2855, 2919, 3423 and 3742 cm^{-1} are observed in both pristine and irradiated samples. The bands at 470 and 564 cm^{-1} are attributed to Y–O stretching vibrations [7,29]. The intensity of these modes decreases with ion irradiation due to loss of crystallinity and/or due to destruction of Y–O stretching bond, which indicates change in chemical composition. The presence of Y–O vibrational bond in irradiated sample signifies its chemical stability after SHI irradiation. Therefore, SHI do not affect the Y–O stretching bond [30]. The band at 740 and 856 cm^{-1} are attributed to the absorption of CO_3^{2-} [31]. The band at 1022 cm^{-1} is attributed to C–O bending and bands at 1407, 1527 and 1703 cm^{-1} are attributed to COO^- group vibration of the citrate complex [32]. The bands at 2919, 3423 and 3742 cm^{-1} are well known and assigned to –OH stretching vibrations [33]. The carbon bonds and OH bands appeared in the FTIR spectra are due to CO_2 and moisture absorbed from the atmosphere [34]. The ligands such as OH–, COO– and CO_3^{2-} are not came from the raw materials used in synthesis and are not observed from the XRD, EDAX techniques. But they are found only in FTIR spectra. Because, the spectra is recorded using KBr pellet technique. KBr is mixed with the samples to make a very thin pellet and the pellet absorbed the CO_2 and moisture present in the atmosphere. Hence, FTIR shows the OH–, COO– and CO_3^{2-} bonds. These results are well reported [20].

Fig. 5(a) shows the IL spectra of pure and Dy^{3+} doped Y_2O_3 and excited with 100 MeV Si^{8+} ions for fluence 0.375×10^{13} ions cm^{-2}. Pure samples do not show IL emission for any of the fluence investigated. A sharp and prominent IL emission with peak at 574 nm is recorded along weak emissions with peaks at

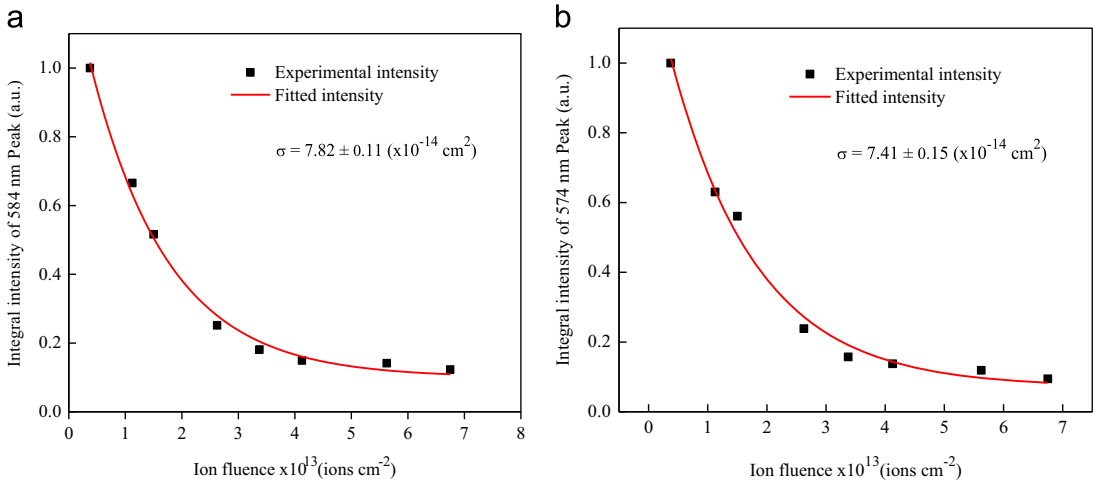

Fig. 7. (a and b) Fitted curves between normalized integral intensity and different fluences of 100 MeV Si ions in Y_2O_3:Dy^{3+}.

488, 584, 670 and 767 nm in Dy^{3+} doped samples. Fig. 5(b) shows the variation of IL intensity for various Dy^{3+} concentrations. It is found that the IL intensity increases with increase of doping concentration and the samples doped with 0.6 mol% exhibits highest intensity in the present investigation.

IL spectra of Y_2O_3:Dy^{3+} (0.6 mol%) nanophosphor bombarded with 100 MeV Si^{8+} ions for the fluence in the range (0.375–6.750) $\times 10^{13}$ ions cm^{-2} are shown in Fig. 6(a). A sharp and prominent IL emission with peak at 574 nm is recorded along with weak emissions at 488, 584, 670 and 767 nm. These characteristic emissions are attributed to the luminescence centers associated with Dy^{3+} ions. Emission peaks at 488, 584 and 670 nm are slightly broadened because of several stark levels of $^4F_{9/2}$ and ^6H_J (J=15/2, 13/2, 11/2) and then split into J+1/2 Stark levels due to Dy^{3+} ion (Kramer's ion) in the lower symmetry site [7]. Similar results on Mg_2SiO_4:Dy^{3+} are reported by Lakshminarasappa et al. [35].

In present work, Dy^{3+} ions are excited by SHI to $^6P_{7/2}$ level and quickly relax non-radiatively to intermediate $^4F_{9/2}$ level. Radiative transition from the intermediate $^4F_{9/2}$ level to the lower states $^6H_{15/2}$, $^6H_{13/2}$, $^6H_{11/2}$ and $^6H_{9/2}$+$^6H_{11/2}$ results in emission with peaks at 488, 574, 670 and 767 nm respectively. The emission with peak at 574 nm corresponds to $^4F_{9/2}\rightarrow{}^6H_{13/2}$ in yellow region which belongs to electric dipole transition and it is allowed only in the case of Dy^{3+} ions. But, it is hypersensitive to the host. Another feeble emission with peak at 488 nm corresponds to the $^4F_{9/2}\rightarrow{}^6H_{15/2}$ (blue region) transition, which belongs to a magnetic dipole transitions and located at the inversion center (C_{3i}) symmetry sites which is less sensitive to the host. Further, weak emissions with peak at 670 nm (Red region) and 767 nm (NIR region) are attributed to $^4F_{9/2}\rightarrow{}^6H_{11/2}$ and $^4F_{9/2}\rightarrow{}^6H_{9/2}$+$^6H_{11/2}$ transitions of Dy^{3+} respectively [7,36]. The IL intensity depends on various factors such as ion species, ion fluence, energy, luminescence activators, quenchers and surrounding environment around the Dy^{3+} ion.

Fig. 6(b) shows the variation of IL integral intensity with ion fluence. It is found that the IL integral intensity decreases rapidly from its initial value and then remains almost constant with increase in ion fluence. The reduction in the IL intensity with increase in ion fluence might be due to distortion of the Y_2O_3:Dy^{3+} crystal lattice. The distortion is enhanced by accumulation of SHI induced defects which provides non-radiative decay path. The decrease in IL intensity may be explained by track interaction model (TIM). According to this model, initially (0.375×10^{13} ions cm^{-2}) SHI ion fluence to create a cylindrical type tracks and such tracks are overlapping each other leadings to the formation of complex defects that reduce the luminescence intensity [37,38].

Further, effective diameter (d) of ion track can be calculated using Poison equation [39,40]. In present work, the diameter of ion tracks is calculated using IL spectra. The cross section (σ) for the damage of the nanophosphor is estimated using the relation

$$I(\varphi) = I_0 \exp(-\sigma\varphi) \quad (4)$$

where σ is the damage cross section of nanophosphor ($\sigma=\pi r^2$), r is the effective radius of ion track, I_0 is the integral intensity of pristine samples, $I(\varphi)$ is the integral intensity of ion irradiation sample, with ion fluence φ. The normalized integrated intensity for Y_2O_3:Dy^{3+} is plotted as a function of ion fluence and shown in Fig. 7(a and b). It is found that, the normalized integrated intensity decreases exponentially with ion fluence. The size of the ion tracks is estimated by fitting this equation and it is found to be 3.10±0.43 and 3.16 ±0.37 nm for 574 and 584 nm emission peaks respectively.

Fig. 8(a) shows the PL excitation spectrum of Y_2O_3:Dy^{3+} recorded in the range 300–400 nm at an excitation of 573 nm. A sharp peak at 349 nm is attributed to the hypersensitive transition $^6H_{15/2}$–$^4M_{15/2}$+$^6P_{7/2}$ and other bands with peaks at 331, 363, 383 nm are attributed to $^6H_{15/2}$–$^4M_{17/2}$, $^6H_{15/2}$–$^4I_{11/2}$ and $^6H_{15/2}$–$^4I_{13/2}$ transitions, respectively [7]. PL emission is recorded under 349 nm excitation. The emission spectra of sol gel derived Y_2O_3:Dy^{3+} nanophosphor irradiated with 100 MeV Si^{8+} ions in the fluence range from 1×10^{10} to 3×10^{11} ions cm^{-2} is shown in Fig. 8(b). The 349 nm (3.6 eV) energy excites the Dy^{3+} ions to the $^6P_{7/2}$ level and then quickly relaxes non-radiatively to intermediate $^4F_{9/2}$ level. After radiative transition from the intermediate $^4F_{9/2}$ level to the lower states, $^6H_{15/2}$, $^6H_{13/2}$ and $^6H_{11/2}$ emitting at 485, 573–583 and 670 nm respectively. The most intense yellow emission at ~573–583 nm corresponds to the hypersensitive transition between the $^4F_{9/2}$ and $^6H_{13/2}$ level of the Dy^{3+} ions. Feorenzo Vetrone et al., reported the spectroscopic investigation of Dy^{3+} doped Y_2O_3 nanocrystal. They observed emission with peaks at 485, 575, 675, 760 and 850 nm which were assigned to the transition from the luminescent $^4F_{9/2}$ level to the ground ^6H_J (J=15/2, 13/2, 11/2, 9/2+11/2 and 7/2+9/2) multiplets [36].

In the present work, 573 nm emission is found to be more intense than at 485 nm emission. The origin of transitions (electric dipole or magnetic dipole) from emitting levels to terminating levels depends upon the site where the Dy ion is located in the Y_2O_3 lattice and the type of transition is determined by selection rules [41]. A Dy^{3+} ion in an Y_2O_3 crystal can occupy two different symmetric sites: (i) a low symmetry site of C_2 without an inversion center and (ii) a high symmetry site of C_{3i} having an inversion center. Y^{3+} ions in unit cell occupy eight sites with C_{3i} point

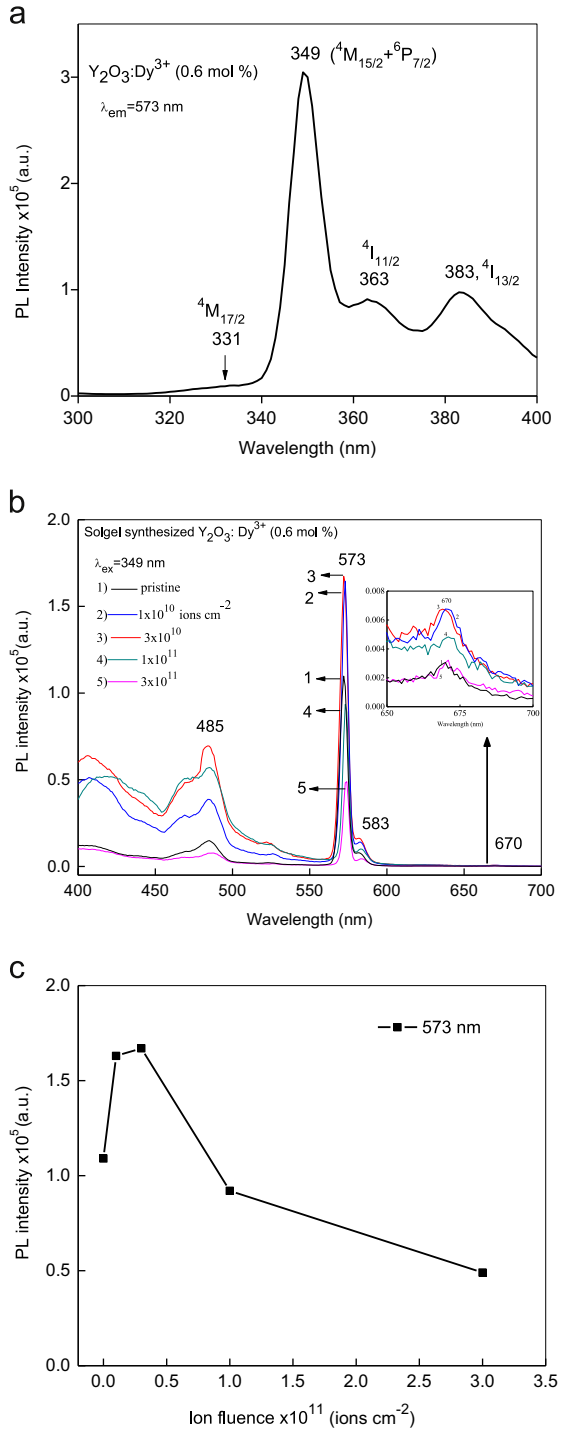

Fig. 8. (a) PL excitation (λ_{em}=573 nm) spectrum of sol gel synthesized nanocrystalline Y_2O_3:Dy^{3+}, (b) PL emission (λ_{ex}=349 nm) spectrum of pristine and 100 MeV swift Si^{8+} ion irradiated Y_2O_3:Dy^{3+} with different ion fluence and (c) Variation of PL intensity with ion fluences.

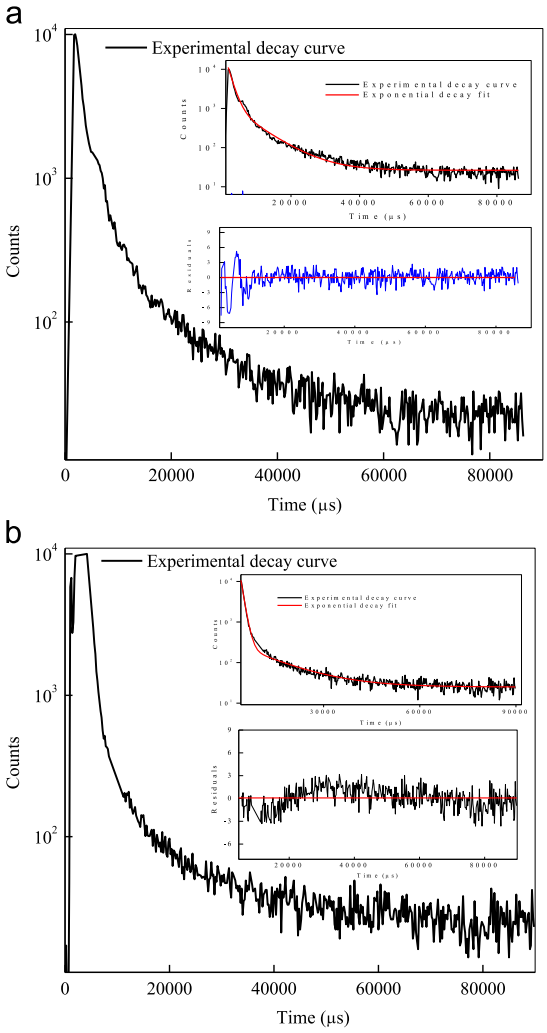

Fig. 9. TRPL decay profile of (a) pristine and (b) 100 MeV swift Si^{8+} irradiated Y_2O_3:Dy^{3+} (0.6 mol%) nanophosphor. The inset shows the lifetime data and the parameters generated by the exponential fitting.

symmetry and 24 sites with C_2 point symmetry. It can be clearly shows that Dy^{3+} occupies the most probability C_2 symmetry in Y_2O_3 lattice [7]. If Dy^{3+} ion occupies the C_{3i} site, the blue (485 nm) emission dominates. And, if Dy^{3+} ions occupy the C_2 site, the yellow (573 nm) emission is dominates. In present work, yellow (573 nm) emission is dominates that of the blue (485 nm) emission, because Dy^{3+} ions are occupied in C_2-site (75%) and C_{3i}-site (25%). It is indicating that the location of the Dy^{3+} is more probability in C_2-site. Therefore, electric dipole (ED) transition ($^4F_{9/2}$–$^6H_{13/2}$) of Dy^{3+} ions is from C_2-sites and magnetic dipole transition ($^4F_{9/2}$–$^6H_{15/2}$) is from C_{3i}-sites. Because, C_{3i}-sites cannot provide odd terms in the crystal field [42,43]. Moreover, the similarity of the ionic radii of Dy^{3+} (~0.91 Å) ions and Y^{3+} (~0.9 Å) ions allows the suitable substitution and C_2-site lacks inversion symmetry. Therefore, Y^{3+} is suitable to substitute Dy^{3+} sites giving rise to intense yellow emission in all the samples [7]. Fig. 8(c) shows variation of PL intensity as a function of ion fluence. The PL intensity at 573 nm is found to increase with increase in ion fluence up to 3×10^{10} ions cm^{-2}, caused due to increase in defects concentration increases in the sample. Further, with increase in ion fluence the PL intensity is found to decrease. And, the decrease in PL intensity at 573 nm might be attributed to the destruction of defects. The disorder leads to crystal field perturbation around Dy^{3+} sites causing inhomogeneous broadening. Nagabhushana et al., reported reduction of PL intensity with increase of Ag^{8+} ion fluence. The decrease in intensity was attributed to the degradation of metal oxide bond. The irradiation effects leads to the restructuring of the surface chemical species due to high energy deposition through electronic energy loss leading to reduction of recombination centers [44].

Time resolved PL (TRPL) is a non destructive technique. The exciton lifetime is an important parameter related to the quality of the material and gives better understanding about quenching mechanism [45]. TRPL decay curves are recorded at room temperature (300 K).

The TRPL decay curves of pristine and SHI irradiated Dy^{3+} doped Y_2O_3 samples measured at 573 nm are shown in Fig. 9(a) and (b), respectively. These decay curves may not fit by a single exponential function due to the nonradiative process involving cross relaxation [46,47]. But it may well be fit by a second order exponential function.

The average lifetime (τ) are found to be 0.96 ± 0.15 ms and 2.31 ± 0.23 ms for pristine and 100 MeV swift Si^{8+} irradiated Y_2O_3:Dy^{3+} nanophosphor. The transition $^4F_{9/2} \rightarrow {}^6H_{13/2}$ (573 nm) is both spin and parity forbidden, hence the life times are long [43,48]. Luminescence of SHI irradiated sample exhibit long decay time (2.31 ms). This might be due to lattice disorder and point defects caused by SHI irradiation. This triggers a partial restructuring of the surface chemical species leading to reduction in nonradiative recombination centers. The decay time results are in consistent with Kiran Sehrawat et al. [49].

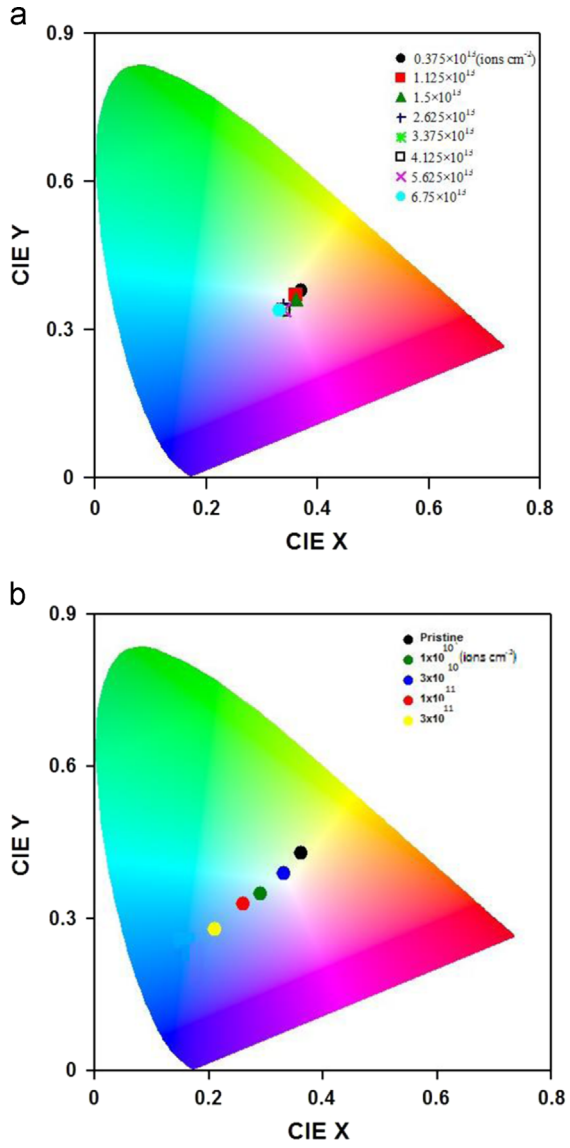

Fig. 10. Color coordinates for 349 nm excitation of (a) IL (b) PL with ion fluence.

3.1. Photometric characterization

To understand the emission of color of the samples more clearly, the Commission Internationale de l'Eclairage (CIE) chromaticity coordinates of pristine and 100 MeV swift Si^{8+} irradiated Y_2O_3:Dy^{3+} (0.6 mol%) for different ion fluences are considered upon 349 nm excitation are calculated from the emission spectra in the range of 400–700 nm using the 1931 CIE system and is shown in Fig. 10(a) and (b), respectively. The calculated color coordinates are tabulated in Table 2. The color coordinates (x–y) of IL are calculated using the standard procedure [20]. The coordinates approaches from closest white region for all the fluence. With increasing ion fluence, (x–y) color coordinates did not changed as shown in Fig. 10(a). Similarly, color coordinates of PL are calculated. The coordinates shifts towards blue region with the increasing ion fluence. This might be due to the destruction of the surface lattice.

4. Conclusions

Y_2O_3:Dy^{3+} nanophosphors are synthesized by sol gel process. The results of XRD and SEM results reveal that the average crystallite size is ~29.67 nm and particles size is 35 nm respectively. The ionoluminescence and photoluminescence spectra of synthesized sample shows the characteristic 5D–4F transitions of Dy^{3+} ion. The decrease in IL intensity is attributed to the destruction of the surface lattice caused by the energy deposited through electronic energy loss and formation of defects leading to non-radiative recombination centers at higher fluences. Time resolved photoluminescence spectroscopy indicated that the PL lifetime is long in irradiated sample. The blue and yellow emissions are varied with ion fluence resulting in the shift of color coordinates from green–yellow to blue region. Thus color tunability can be achieved by changing the ion fluences. Present investigations indicated that Y_2O_3:Dy^{3+} nanophosphor is a promising candidate for applications in optoelectronic devices and solid state lighting for general illumination purposes.

Table 2
CIE parameters of pristine and ion irradiated Y_2O_3:Dy^{3+} nanophosphor.

Technique	Ion fluence ($\times 10^{13}$ ions cm^{-2})	Color coordinates		Technique	Ion fluence (ions cm^{-2})	Color coordinates	
		x	y			x	y
IL	0.375	0.37	0.38	PL	Pristine	0.36	0.43
	1.125	0.36	0.37		1×10^{10}	0.29	0.35
	1.50	0.36	0.36		3×10^{10}	0.33	0.39
	2.625	0.34	0.34		1×10^{11}	0.26	0.33
	3.375	0.34	0.34		3×10^{11}	0.21	0.28
	4.125	0.34	0.34				
	5.625	0.34	0.34				
	6.75	0.33	0.34				

Acknowledgments

The authors express their sincere thanks to Dr. D.K. Avasthi, Materials Science Group, Dr. S.P. Lochab, Health Physics Group, Inter University Accelerator Center, New Delhi, India and Dr. D. Haranath, Luminescent Materials and Devices Group, National Physical Laboratory, New Delhi, India for their constant encouragement and help during the experiment. Also, one of the authors (NJS) is grateful to Inter University Accelerator Center, New Delhi, for providing fellowship under UFR (No. 48303) scheme.

References

[1] N. Itoh, D.M. Duffy, S. Khakshouri, M. Stoneham, J. Phys. Condens. Matter 21 (2009) 474205.
[2] J.F. Zeigler, J.P. Biersack, U. Littmark, Stopping and Range of Ions in Solids, Pergamon Press, New York, 1985.
[3] M. Toulemonde, J.M. Constantini, Ch Dufour, A. Meftah, E. Paumier, F. Studer, Nucl. Instrum. Methods Phys. Res. Sect. B: Beam Interact. Mater. Atoms 116 (1996) 37.
[4] M. Toulemonde, S.M.M. Ramos, H. Bernas, C. Clerc, B. Canut, J. Chaumont, C. Trautmann, Nucl. Instrum. Methods Phys. Res. Sect. B: Beam Interact. Mater. Atoms 178 (2001) 331.
[5] Yufeng Song, Qi Liu, Youmei Sun, Jie Liu, Zhiyong Zhu, Nucl. Instrum. Methods Phys. Res. Sect. B Beam Interact. Mater. Atoms 254 (2007) 268.
[6] V. Dubey, J. Kaur, S. Agrawal, Res. Chem. Intermed. 41 (2015) 4727.
[7] M. Jayasimhadri, B.V. Ratanam, Kiwan Jang, Ho Sueb Lee, Baojiu Chen, Soung-Soo Yi, Jung-Hyun Jeong, L. Rama Moorthy, J. Am. Ceram. Soc. 93 (2010) 494.
[8] H. Calvo del Castillo, J.L. Ruvalcaba, T. Calder´on, Anal. Bioanal. Chem. 387 (2007) 869.
[9] H. Calvo del Castillo, A. Millan, P. Beneıtez, J.L. Ruvalcaba-Sil, T. Calderon, Rev. Mex. Fis. 54 (2008) 93.
[10] J.L. Ruvalcaba-Sil, L. Manzanilla, E. Melgar, R. Lozano Santa Cruz, X-Ray Spectrom. 37 (2008) 96.
[11] H. Calvo del Castilloa, J.L. Ruvalcabab, M. Bettinellic, A. Speghinic, M. Barboza Floresd, T. Calderona, D. Jaquee, J. Garcia Sole, J. Lumin. 128 (2008) 735.
[12] H. Nagabhushana, B. Umesh, B.M. Nagabhushana, B.N. Lakshminarasappa, F. Singh, R.P.S. Chakradhar, Philos. Mag. 89 (2009) 995.
[13] A. Dupont, C. Parent, B. Le Garrec, J. Heintz, J. Solid State Chem. 171 (2003) 152.
[14] B.N. Lakshminarasappa, N.J. Shivaramu, K.R. Nagabhushana, Fouran Singh, Nucl. Instrum. Methods Phys. Res. Sect. B: Beam Interact. Mater. Atoms 329 (2014) 40.
[15] Li Chen Weifan, Liu Fengsheng, Yongxiu Leili, J. Rare Earths 24 (2006) 543.
[16] Shibani Das, Study of Composition Behavior of Binders and the Effect of Bender Type on Strength and Density of Alumina Samplesk (B. Tech. thesis), National institute of Technology, Rourkela (2011), p. 26–27.
[17] D. Kanjilal, S. Chopra, M.M. Narayanan, S. Iyer Indira, R.J.J. Vandana, S.K. Datta, Nucl. Instrum. Methods Phys. Res. A 328 (1993) 97.
[18] N. Salah, P.D. Sahare, J. Phys. D: Appl. Phys. 39 (2006) 2684.
[19] J.F. Ziegler, Nucl. Instrum. Methods Phys. Res. Sect. B: Beam Interact. Mater. Atoms 268 (2010) 1818.
[20] S. Som, S. Dutta, V. Kumar, V. Kumar, H.C. Swart, S.K. Sharma, J. Lumin. 146 (2014) 162.
[21] Tong Liu, Wen Xu, Xue Bai, Hongwei Song, J. Appl. Phys. 111 (2012) 064312.
[22] R.J. Gaboriaud, M. Jublot, F. Paumier, B. Lacroix, Nucl. Instrum. Methods Phys. Res. Sect. B: Beam Interact. Mater. Atoms 310 (2013) 6.
[23] S. Hemon, V. Chailley, E. Dooryhée, C. Dufour, F. Gourbilleau, F. Levesque, E. Paumier, Nucl. Instrum. Methods Phys. Res. Sect. B: Beam Interact. Mater. Atoms 122 (1997) 563.
[24] Zhiyong Youmei Sun, Zhiguang Zhu, Jie Wang, Yunfan Liu, Mingdong Jin, Ying Hou, Jinglai Wang, Duan, Nucl. Instrum. Methods Phys. Res. Sect. B: Beam Interact. Mater. Atoms 212 (2003) 211.
[25] A. Vij, R. Kumar, A.K. Chawla, S.P. Lochab, R. Chandra, N. Singh, Opt. Mater. 33 (2010) 58.
[26] B.D. Cullity, Elements of X-Ray Diffraction, 2nd ed., Addison–Wesley Publishing Company, Inc., USA, 1956.
[27] Rene Guinebretière, X-ray Diffraction by Polycrystalline Materials, Antony Rowe Ltd., Chippenham, Wiltshire. Great Britain, 2007.
[28] S. Som, M. Chowdhury, S.K. Sharma, J. Mater. Sci. 49 (2013) 858.
[29] B.N. Lakshminarasappa, J.R. Jayaramaiah, B.M. Nagabhushana, Powder Technol. 217 (2012) 7.
[30] K.R. Nagabhushana, B.N. Lakshminarasappa, G.T. Chandrappa, D. Haranath, F. Singh, Radiat. Eff. Defects Solids 162 (2007) 325.
[31] J.F.S. Bitencourt, K.A. Goncalves, S.H. Tatumi, P.J.B. Marcos, J. Phys. Conf. Ser. 249 (2010) 012052.
[32] B. Van Hao, P.T. Huy, T.N. Khiem, N.T.T. Ngan, P.H. Duong, J. Phys. Conf. Ser. 187 (2009) 012074.
[33] R.V. Mangalaraja, J. Mouzon, P. Hedstrom, P. Camurri, S. Carlos, M. Oden Ananthakumar, Powder Technol. 191 (2009) 309.
[34] Faheem Ahmed, Shalendra Kumar, Nishat Arshi, M.S. Anwar, Bon Heun Koo, Chan Gyu Le, Microelectron. Eng. 89 (2012) 129.
[35] B.N. Lakshminarasappa, S.C. Prashantha, F. Singh, Curr. Appl. Phys. 11 (2011) 1274.
[36] F. Vetrone, J.C. Boyer, J.A. Capobianco, A. Speghini, M. Bettinelli, Nanotechnology 15 (2004) 75.
[37] G. Szenes, Phys. Rev. B 60 (1999) 3140.
[38] V.A. Skuratov, K.J. Gun, J. Stano, D.L. Zagorski, Nucl. Instrum. Methods Phys. Res. Sect. B: Beam Interact. Mater. Atoms 245 (2006) 194.
[39] S.K. Gautam, F. Singh, I. Sulania, R.G. Singh, P.K. Kulriya, E. Pippel, J. Appl. Phys. 115 (2014) 143504.
[40.] R. Singhal, F. Singh, a Tripathi, D.K. Avasthi, Radiat. Eff. Defects Solids 164 (2009) 38.
[41] M. Yen William, Shigeo Shionoya, Hajime Yamamoto, Phosphor Handbook, 2nd ed., CRC Press Taylor & Francis Group, New York, 2007.
[42] A. Tanner, C.K. Duan, Coord. Chem. Rev. 254 (2010) 3026.
[43] Guifang Ju, Yihua Hu, Li Chen, Xiaojuan Wang, Zhongfei Mu, Haoyi Wu, Fengwen Kang, J. Lumin. 132 (2012) 1853.
[44] H. Nagabhushana, S.C. Prashantha, B.N. Lakshminarasappa, F. Singh, J. Lumin. 128 (2008) 7.
[45] B.K. Gupta, D. Haranath, S. Saini, V.N. Singh, V. Shanker, Nanotechnology 21 (2010) 055607.
[46] K.B. Eisenthal, S. Siegel, J. Chem. Phys. 41 (1964) 652.
[47] M. Inokuti, F. Hirayama, J. Chem. Phys. 43 (1978) 1965.
[48] Dhiraj K. Sardar, William M. Bradley, Raylon M. Yow, John B. Gruber, Bahram Zandi, J. Lumin. 106 (2004) 195.
[49] Kiran Sehrawat, Fouran Singh, B.P. Singh, R.M. Mehra, J. Lumin. 106 (2004) 21.